Biophysical Journal, Volume *112*

Supplemental Information

Heterogeneous Tau-Tubulin Complexes Accelerate Microtubule Polymerization

Xiao-Han Li and Elizabeth Rhoades

Materials and Methods

Tau expression, purification and labeling

The sequence of tau P1234R' was cloned into a pET-HT vector with an N-terminal His-tag and a tobacco etch virus (TEV) cleavage site for removal of the His-tag. Stepwise truncations of P1234R' to produce P1234, P123IR$_{3/4}$, P123, P12IR$_{2/3}$ and P12 were performed by insertion of stop codons at the appropriate positions. P134R' was created via overlap extension PCR to remove IR$_{1/2}$-R2 from the P1234R' sequence. Stepwise truncations of P134R' to produce P134, P13IR$_{3/4}$ and P13 were accomplished by insertion of stop codons. P1324 was created by insertion of IR$_{1/2}$-R2 into the P134 sequence between repeat 3 and inter-repeat 3/4, and P132 was created by inserting a stop codon by the end of repeat 2 in P1324. P124 was created by overlap extension to remove IR$_{2/3}$-R3. P1234* was created by overlap extension using P124 as template. For site-specific labeling of tau constructs, the endogenous cysteines at residues 291 and 322 were mutated to serines and a serine to cysteine mutation was introduced by site directed mutagenesis at residue 198. The introduction of stop codons and site-directed mutagenesis utilized a QuikChange Site-Directed Mutagenesis Kit (Agilent Technologies). All the overlap extension PCR utilized Phusion-HF polymerase (New England Biolabs).

Tau constructs were expressed in *E. coli* and purified as previously reported (1). Briefly, *E. coli* transformed with a desired plasmid were grown in 500 mL LB media incubated at 37 ℃ with shaking until OD$_{600}$=0.4–0.6. Protein expression was induced by the addition of 1.6 mM IPTG with growth overnight at 16 ℃. The cells were collected by centrifugation at 5,000xg at 4 ℃ for 30 minutes and the supernatant was discarded. The cell pellets were lysed by ultrasonication in 15 mL lysis buffer (50 mM Tris, pH 8, 500 mM NaCl, 10 mM imidazole) with 1 mg/mL lysozyme, 1 tablet of Complete Mini EDTA-free protease inhibitor cocktail (Roche) and 1 mM PMSF added. Lysed cells were centrifuged at 20,000xg to remove cell debris. The supernatant was filtered through a 0.22 μm syringe filter and then incubated with Ni-NTA agarose (QIAGEN) for ~1 hour at 4 ℃ with gentle mixing. The column material was washed with 60mL Ni-NTA buffer A (50 mM Tris, pH 8, 500 mM NaCl, 10 mM imidazole). The protein was eluted in a single step with Ni-NTA buffer B (50 mM Tris pH 8, 500 mM NaCl, 400 mM imidazole). The eluted protein solution was concentrated to ~1 mL and the His-tag was removed by overnight incubation at 4 ℃ with TEV in the presence of 1 mM DTT. The cleaved sample was buffer-exchanged back into Ni-NTA buffer A and again passed over the Ni-NTA agarose to remove His-tagged TEV, cleaved His-tags and uncleaved tau. Final purification was by size-exclusion chromatography using a Superdex-200 column (GE HiLoad 16/600) in SEC buffer (25 mM Tris pH 8, 100 mM NaCl, 1 mM EDTA, 0.5 mM TCEP). The fractions containing tau were combined and concentrated. The cysteine mutants were labeled immediately; constructs used for polymerization assays were flash-frozen and stored at -80 ℃ until needed.

For FCS measurements, tau was labeled with Alexa 488 maleimide (Life Technologies). 200 μL of approximately 500 μM protein in SEC buffer was treated with 1 mM DTT at room temperature for 30 minutes. The solution was passed through two coupled desalting columns (GE, HiTrap) to remove DTT and to buffer exchange into labeling buffer (20 mM Tris pH 7.4, 50 mM NaCl, 6 M GdnHCl). After exchange, ~4x Alexa 488 maleimide (Life Technologies) dissolved in anhydrous DMSO was titrated into the protein solution stepwise with stirring, taking

care that the final DMSO concentration did not exceed 1%. The reaction mixture was incubated in the dark at room temperature for 30 minutes and then 4 ℃ overnight with stirring. To remove unreacted dye and buffer exchange the labeled protein, the sample was passed over two coupled desalting columns (GE, HiTrap) equilibrated with storage buffer (20 mM Tris pH 7.4, 50 mM NaCl) before aliqouting and flash freezing for storage at -80 ℃. All constructs appear to be >95% labeled as only a single peak with mass corresponding to single-labeled protein was observed by MALDI mass spectrometry for each construct.

DARPin and RB3 purification and labeling

DARPin and RB3 were expressed and purified as described previously (1,2). Briefly, 1 L of *E. coli* cells expressing either DARPin or RB3 were lysed by ultrasonication in 30 mL lysis buffer. After removing cell debris by centrifugation at 20000xg , the homogenate was filtered through a 0.22 μm syringe filter and then incubated with Ni-NTA agarose (QIAGEN) for ~1 hour at 4 ℃ with gentle shaking. The column material was washed with 60 mL Ni-NTA buffer A. The protein was eluted in a single step with Ni-NTA buffer B. For DARPin purification, the protein was further purified by a Superdex-200 column (GE HiLoad 16/600) run in SEC buffer. For RB3 purification, the elution was concentrated to 1 mL and treated with TEV in the presence of 1 mM DTT at 4 ℃. The cleaved sample was exchanged back into Ni-NTA buffer A and then passed over the Ni-NTA agarose to remove His-tagged TEV, cleaved His-tags and uncleaved RB3. Finally, RB3 was purified by a Superdex-200 column (GE HiLoad 16/600) run in SEC buffer. Both DARPin and RB3 were labeled with Alexa 488 maleimide (Life Technologies) using the same method as described for tau, but in the absence of 6 M GdnHCl. The labeled proteins were aliquoted and flash frozen for storage at -80 ℃ until use.

Tubulin purification, labeling and general handling

Tubulin was purified from bovine brains following a published protocol (3). Briefly, fresh bovine brains were cleared of blood vessels and homogenized in a cold depolymerization buffer (50 mM MES, 1 mM $CaCl_2$, pH 6.6). The homogenate was clarified by ultracentrifugation, and supernatant containing tubulin was further purified through two cycles of warm polymerization with glycerol followed by cold depolymerization. The purity of the resulting tubulin was verified by SDS-PAGE. Finally, the purified tubulin was aliquoted and flash-frozen in liquid nitrogen for storage at -80 ℃. For FCS measurements requiring fluorescently labeled tubulin, freshly purified tubulin was labeled with Alexa 488 according to published protocols (4).

For use, tubulin aliquots were thawed quickly and immediately placed on ice. The thawed samples were clarified by centrifugation at 98,000xg for 6 minutes at 4 ℃. For polymerization assays, the clarified tubulin was kept on ice in BRB80 buffer (80 mM PIPES, 1 mM $MgCl_2$, 1 mM EGTA) prior to use. For FCS measurements, clarified tubulin was buffer exchanged into phosphate buffer (20 mM potassium phosphate pH 7.4, 20 mM KCl, 1 mM $MgCl_2$, and 0.5 mM EGTA with 1 mM DTT freshly added) via a Biospin 6 column (Bio-Rad) prior to use. The

tubulin concentration was determined by absorption at 280 nm using an extinction coefficient of 115,000 $M^{-1}cm^{-1}$ on a Nanodrop 2000 (Thermo Fisher).

To avoid the well-known issues of variability between tubulin samples (5,6), tubulin used in these experiments came from a single purification of bovine tubulin. We do note that a subset of the measurements was also carried out using tubulin from a separate purification. We found that the absolute diffusion times of tau-tubulin complexes differed slightly for tubulin from different preparations. However, the trends in median values as well as the relationship between specific constructs and heterogeneity in the FCS curves were all consistent with the detailed results reported here.

Fluorescence correlation spectroscopy (FCS)

FCS measurements were performed on a lab-built instrument based on an inverted Olympus microscope similar to described previously (1). The laser power was adjusted to 4.5–5.5 μW as measured prior to entering the microscope. Fluorescence emission was collected through the objective (Olympus) and separated from excitation using a Z488RDC long pass dichroic and an HQ600/200M bandpass filter (Chroma). The emission was focused onto the aperture of an optical fiber (OzOptics) with a diameter of 50 μm directly coupled to an avalanche photodiode (Perkin-Elmer). A digital correlator (Correlator.com) was used to generate the autocorrelation curves.

Measurements were made in 8-well Nunc chambers treated with PEG-PLL to prevent non-specific adsorption of the proteins (7). All FCS measurements were made at 20 ℃ in phosphate buffer and in the absence of GTP, conditions which disfavor polymerization. This buffer was chosen because tubulin binding by tau, DARPin, and RB3 are all observed and it allows for comparison with prior studies (1,2). Polymerization assays were carried out using the same buffer conditions of the FCS measurements to verify that no polymerization was observed (**Fig. S2**). FCS measurements of tau in solution were made using ~20 nM tau and twenty, 10-second autocorrelation curves were obtained for each sample. The curves were averaged and analyzed as described below. For FCS measurements of tau (or DARPin or RB3) bound to tubulin, 20 nM of the labeled construct was mixed with 20 μM of unlabeled tubulin and incubated for 5 minutes at 20 ℃ prior to measurement. This concentration of tubulin was chosen based on FCS measurements of P12 and P13 which showed no increase in diffusion time between 20 μM and 30 μM tubulin. For measurements with excess tau, 20 nM of labeled tubulin was mixed with 20 μM unlabeled tau and incubated for 5 minutes prior to measurement. At least 100 individual autocorrelation traces of 10 second each were collected over at least two days of measurements and analyzed as described below.

FCS analysis

For analysis of the FCS measurements of tau in solution, the average autocorrelation curve, $G(\tau)$ was fit to an equation modeling 3D diffusion of a single fluorescent species (Eq. S1)

$$G(\tau) = \frac{1}{N}\left(1+\frac{\tau}{\tau_D}\right)^{-1}\left(1+\frac{s^2\tau}{\tau_D}\right)^{-\frac{1}{2}} \quad \text{(Eq. S1)}$$

where N is the average number of fluorescent molecules, τ_D is the mean diffusion time of labeled protein, s is the ratio of the radial to axial dimensions of the focal volume, determined to be 0.2 for our system and fixed for analysis. The reported diffusion times are the average and standard deviation of independent measurements taken on at least three different days. The average brightness of the construct (utilized in the analysis described below) was calculated by dividing the average total intensity of the measurement by N derived from the fit. This data was also analyzed by the method developed for analysis of FCS data from tau-tubulin complexes (described below). For the measurements of tau in solution, the diffusion times determined by these two approaches (analyzing averaged versus individual curves) are, as expected for homogenous samples, in very good agreement (**Table S1**).

FCS measurements of heterogeneous complexes observed using labeled tau fragments in an excess of unlabeled tubulin resulted in autocorrelation curves that did not overlie each other (**Fig. S1**) and thus were not amenable to traditional FCS analysis as described above. To address this, we devised an analysis which allowed us to quantify the heterogeneity of the complexes. The challenge faced analysis is how to quantify heterogeneity while not allowing our analysis to be dominated by very bright and large – although infrequent – tau-tubulin assemblies. Each individual autocorrelation curve was fit to the 3D single-component diffusion model given in Eq. S1 to extract the diffusion time and molecular brightness. The molecular brightness for each construct bound to tubulin was divided by the molecular brightness of the same construct in solution measured on the same day. This allows us to account for day-to-day variances in laser intensity and alignment, as well as any variability in the intrinsic brightnesses of the constructs. The distribution of molecular brightness after normalization for each construct was fit to a Gaussian distribution. Any points lying outside the mean ±1.96 σ of the Gaussian fit were treated as outliers of the major population and were discarded (**Fig. S7** and **Fig. S8**). These boundaries represent a 95% of confidence interval of the Gaussian. This procedure was done iteratively until no additional events were discarded (**Fig. S7**). This part of the fitting process eliminated very bright assemblies which dominate the autocorrelation curve, despite representing a small fraction of the assemblies in the samples.

The remaining autocorrelation curves were fit with Eq. S1 and R-squared of the fit was calculated between 0.01–1000 ms. Any curve with R-squared < 0.99 was discarded (**Fig. S9**). This process ensures a single diffusion time accurately reflects the average size of the distribution of tau-tubulin assemblies present in the sample. **Figs. S10 and S11** shows the average brightness and median diffusion times and their associated peak widths for the Gaussian distribution fit to the diffusion times, respectively, for all the constructs before and after our filtering analysis. While the absolute values of diffusion times and widths change (**Fig. S11**), the relative trends between the constructs are conserved through our analysis. Moreover, these plots show that the inclusion of all curves would actually make our findings more dramatic – i.e. results further delineation of multiple tubulin binders from stoichiometric one; however, we erred on the side of caution to avoid over-interpretation of infrequent events. In other words, the

combination of 'brightness' filtering with goodness-of-fit to a one-component model results in a conservative estimate of the heterogeneity of the tau-tubulin assemblies.

We chose to use a single component diffusion model to fit the data because of concern that multi-component models would over-parameterize the fitting equations. In a rather simple case where tau binds to either one or two tubulin dimers, the diffusion times of these two complexes is expected to vary by ~1.2x, as estimated by comparing between DARPin-tubulin and RB3-tubulin complexes. Differentiating between any two different diffusing species in solution with a two-component fit equation generally requires at least a 1.6x difference in their diffusion times (8). Thus, the diffusion times extracted from a two-component fit would not be robust. For cases with more variable stoichiometry in the tau-tubulin complexes – the more probable case for the measurements here – meaningful fitting with multiple components becomes even more challenging.

To quantify and compare between constructs, we report the median diffusion times and FWHM (2.355σ) widths from a Gaussian distribution fit to the diffusion times as described above (columns 3 and 4 of **Table 1**). For comparison with simple averaging of the diffusion times, we report both the parameters of the Gaussian fit as well as the arithmetic medians and standard deviations in **Table S3**. These are in very good agreement. For presentation and discussion of our data, we chose to use the Gaussian fit parameters as they are less influenced by outliers.

Heterogeneity in filtered data: analysis of time traces

Even after the filtering method described above, there was still significant heterogeneity in the diffusion times of tau-tubulin complexes for many of the constructs. To determine the origin of this heterogeneity, photon burst detection experiments were performed on one construct displaying significant heterogeneity (P1234R') and one with minimal heterogeneity (P13). For each construct, 30–50 traces of 10 seconds each were taken of 20 nM labeled protein in the absence or presence of 20 μM unlabeled tubulin. Time traces were recorded by an avalanche photon detector with photon binning time of 400 μs with autocorrelation curves calculated simultaneously. After completing a tau-tubulin measurement, 500 mM KCl was added to the samples and they were re-measured. The autocorrelation curves were fit to a single-component diffusion model as described before and datasets of tau-tubulin were subject to Gaussian filtering (as described above) before further analysis to remove very bright species.

For data analysis, every 5 adjacent time bins were further grouped together to decrease the effect of noise so the final temporal resolution is 2 ms. The average number of photons in each bin, μ, and standard deviation, σ, of each 10 second trace were determined and used to calculate *z*, which reflects the deviation of the number of photons in a bin compared to the mean value, as a standardized indicator for photon bursts (Eq. S2)

$$z = \frac{x - \mu}{\sigma} \quad \text{(Eq. S2)}$$

where μ and σ are defined above and *x* is the number of photons in an individual bin.

As can be seen in the traces of P1234R' (**Fig. S5**), occasional sampling of brighter species, appears as 'bursts' can be observed in the presence of tubulin. Such bursts are not present in traces of tau in the absence of tubulin or after the addition of 500 mM KCl to tau-tubulin samples. This suggests that the observed species are tubulin-dependent and reversible. Moreover, such bursts were rarely observed for P13-tubulin which has a small variance in diffusion times (**Fig. S6**).

Bursts were identified by varying the photon count/bin threshold over $\mu + 3\sigma$, 4σ or 5σ for the bin sizes of either 400 μs or 2 ms. Based on this criteria, the burst frequency is ~0.2–0.6 s^{-1} or every ~2–6 bursts per 10 second autocorrelation curve.

Microtubule polymerization assay

Microtubule polymerization assays were performed as described previously (9) by monitoring an increase in scattered light. Briefly, 15 μM tau and 30 μM tubulin were mixed on ice in degassed BRB80 with 1 mM fresh DTT. 3 mM GTP was added, the sample was briefly mixed, and immediately transferred to a quartz cuvette (Starna Cells, Inc.) preincubated at 37 ℃. Polymerization was monitored by an increase of light scattering at 350 nm on a fluorimeter (PTI technologies) with slit widths for excitation and emission both set to 5 nm. The reaction was followed until a plateau in the scattering signal was reached. The resulting curves were normalized and fit to a sigmoidal equation (Eq. S3):

$$y = \frac{1}{1 + e^{\frac{t - t_{1/2}}{dt}}} \quad \text{(Eq. S3)}$$

where $t_{1/2}$ is the polymerization half-time, dt is the time constant. The pseudo-first-order rate constant, $k_{obs} = 1/t_{1/2}$ was also used to quantify polymerization.

Sequence analysis

Sequences for R1, R2, R3, R4 and R' were analyzed by CIDER online (10) to extract charge profile of these domains. The results reported here contains fraction of charged residues (FCR), net charge per residue (NCPR), and κ. The FCR is calculated from dividing the number of charged residues (lysine, arginine, glutamate, aspartate) by the total number of residues in a sequence; the NCPR is calculated from dividing the net charge a sequence carries by the number of residues. FCR and NCPR reflect general electrostatic property of a sequence. κ describes the charge segregation of the sequence, as a quantity describing how well the positive and negative charges in a sequence are separated. A low κ represents a system where positively charged residues and negatively charged residues are well mixed. See work from Das and Pappu (11) for more details.

Table S1 Diffusion times for tau constructs and controls in solution

Construct	diffusion time (average)[a] (mean ± std) (ms)	diffusion time (individual)[b] (median ± std) (ms)
P1234R'	0.55 ± 0.02	0.56 ± 0.03
P1234	0.51 ± 0.02	0.51 ± 0.03
P123IR$_{3/4}$	0.46 ± 0.01	0.46 ± 0.02
P123	0.43 ± 0.01	0.43 ± 0.02
P12IR$_{2/3}$	0.41 ± 0.01	0.41 ± 0.04
P12	0.39 ± 0.01	0.39 ± 0.02
P134R'	0.51 ± 0.01	0.51 ± 0.02
P134	0.44 ± 0.01	0.44 ± 0.02
P13IR$_{3/4}$	0.44 ± 0.01	0.44 ± 0.02
P13	0.39 ± 0.01	0.39 ± 0.02
P124	0.45 ± 0.01	0.45 ± 0.02
P1324	0.49 ± 0.01	0.49 ± 0.02
P132	0.46 ± 0.02	0.46 ± 0.04
P1234*	0.50 ± 0.01	0.50 ± 0.02
DARPin	0.31 ± 0.01	0.31 ± 0.01
RB3	0.33 ± 0.01	0.33 ± 0.02

[a] The reported diffusion times are the results of fitting averaged curves (20 individual curves averaged per measurement) from at least three separate measurements. The mean and standard deviation are calculated from the fit parameters of the separate measurements.
[b] The reported diffusion times are calculated from the same datasets as in the middle column; each curve is fit individually and the reported values are the arithmetic medians and standard deviations from these individual fits.

Table S2 Charge distribution of sequences of subdomains of tau

subdomain	sequence	FCR	NCPR	κ
R1	QTAPVPMPDLKNVKSKIGSTENLKHQPGGGK	0.23	0.10	0.24
R2	VQIINKKLDLSNVQSKCGSKDNIKHVPGGGS	0.23	0.10	0.16
R3	VQIVYKPVDLSKVTSKCGSLGNIHHKPGGGQ	0.16	0.10	0.21
R4	VEVKSEKLDFKDRVQSKIGSLDNITHVPGGGN	0.31	0	0.07
R'	KKIETHKLTFRENAKAKT	0.44	0.22	0.08

Charge distribution of sequences of R1, R2, R3, R4 (including inter-repeats) and the conserved sequence of R' with positive residues in blue and negative residues in red. The conserved sequences within repeats are underlined. R' has a higher fraction of charged residues (FCR), net charge per residue (NCPR), with a small κ compared to R1, R2 and R3.

Table S3 Diffusion times for tau constructs and controls in the presence of tubulin

	construct	median diffusion time (ms)		standard deviation σ (ms)	
		arithmetic	Gaussian fit	arithmetic	Gaussian fit
4R	P1234R'	0.88	0.87	0.15	0.14
	P1234R' (excess tau)	0.67	0.67	0.04	0.04
	P1234	0.76	0.75	0.09	0.06
	$P123IR_{3/4}$	0.67	0.67	0.05	0.05
	P123	0.69	0.69	0.06	0.05
	$P12IR_{2/3}$	0.64	0.63	0.06	0.04
	P12	0.61	0.60	0.04	0.03
	P12 (excess tau)	0.61	0.61	0.03	0.04
3R	P134R'	0.80	0.79	0.10	0.10
	P134	0.66	0.65	0.05	0.04
	$P13IR_{3/4}$	0.66	0.66	0.05	0.04
	P13	0.60	0.60	0.05	0.04
	P13 (excess tau)	0.60	0.60	0.03	0.03
scrambled	P1324	0.75	0.74	0.08	0.06
	P1234*	0.76	0.76	0.07	0.05
	P132	0.73	0.72	0.09	0.06
	P124	0.65	0.65	0.04	0.04
controls	DARPin	0.60	0.60	0.03	0.03
	RB3	0.73	0.73	0.04	0.04
	tubulin	0.53	0.52	0.03	0.04
	tubulin (20μM)	0.54	0.54	0.03	0.03

The parameters reported are from either arithmetic statistics (columns 1 and 3) or a Gaussian distribution fit (columns 2 and 4) of the individual autocorrelation curves. The median and σ are nearly identical. The data reported in **Table 1** corresponds to the median diffusion time and the peak width, 2.355σ of the Gaussian fit.

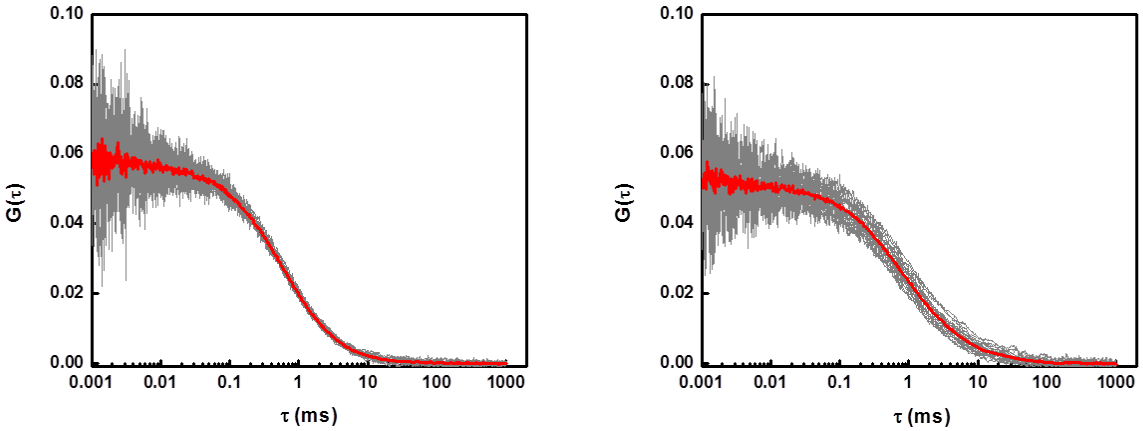

Figure S1 Representative FCS curves for P1234R' in the absence (left) and presence (right) of 20 μM tubulin. Individual autocorrelation curves are in gray. The red line is the average of the 20 autocorrelation curves.

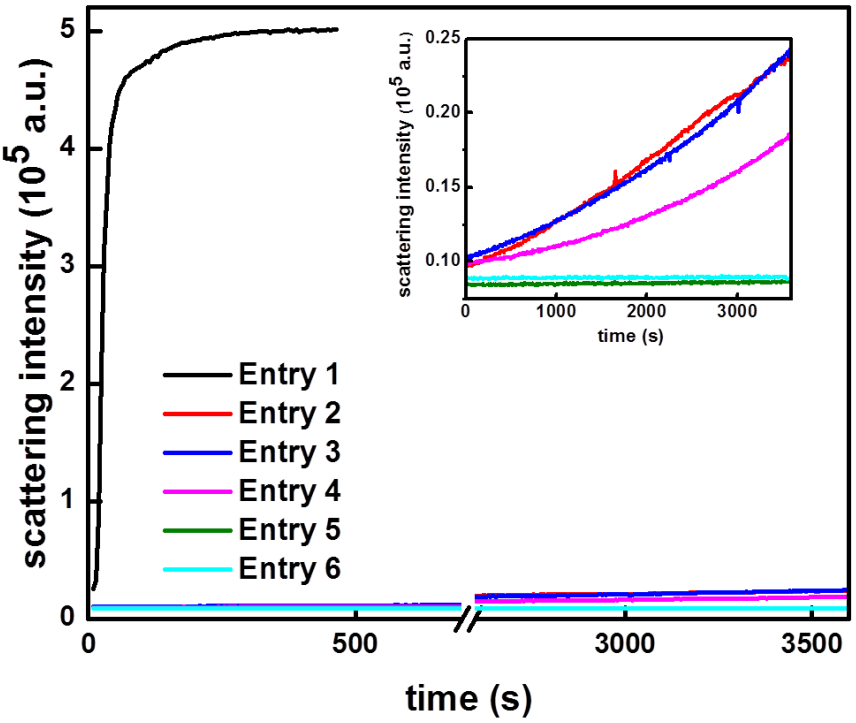

entry	buffer	P1234R'	tubulin	GTP	temperature
1	BRB80	15 μM	30 μM	3 mM	37 ℃
2	BRB80	20 nM	30 μM	3 mM	37 ℃
3	BRB80	20 nM	30 μM	none	37 ℃
4	BRB80	none	30 μM	none	37 ℃
5	phosphate	20 nM	20 μM	none	20 ℃
6	phosphate	none	20 μM	none	20 ℃

Figure S2 Tau does not promote microtubule polymerization under conditions of FCS measurements. Tubulin polymerization was monitored by light scattering as described in the text for various conditions as detailed in the table. Entry 1 is polymerization under typical conditions. For conditions comparable to the to the FCS measurements (Entry 5), polymerization is not observed.

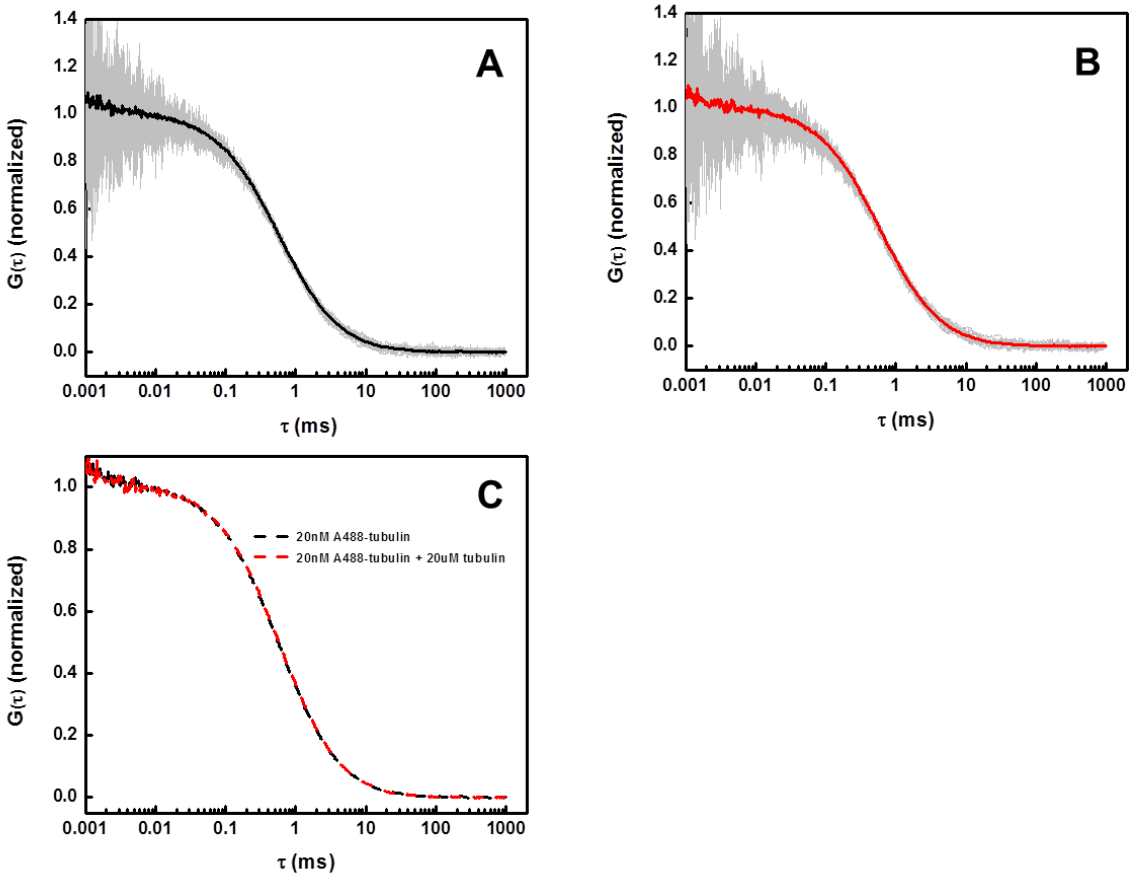

Figure S3 Tubulin does not oligomerize under FCS conditions. Normalized FCS curves (gray) of 20 nM Alexa 488 tubulin in the absence (A) and presence (B) of 20 μM unlabeled tubulin, respectively, were plotted. The average curve for each measurement is overlapped with the 20 individual curves. Panel C plots the two average curves and shows that they are superimposable. There is no evidence of concentration-dependent oligomerization of tubulin in the absence of tau.

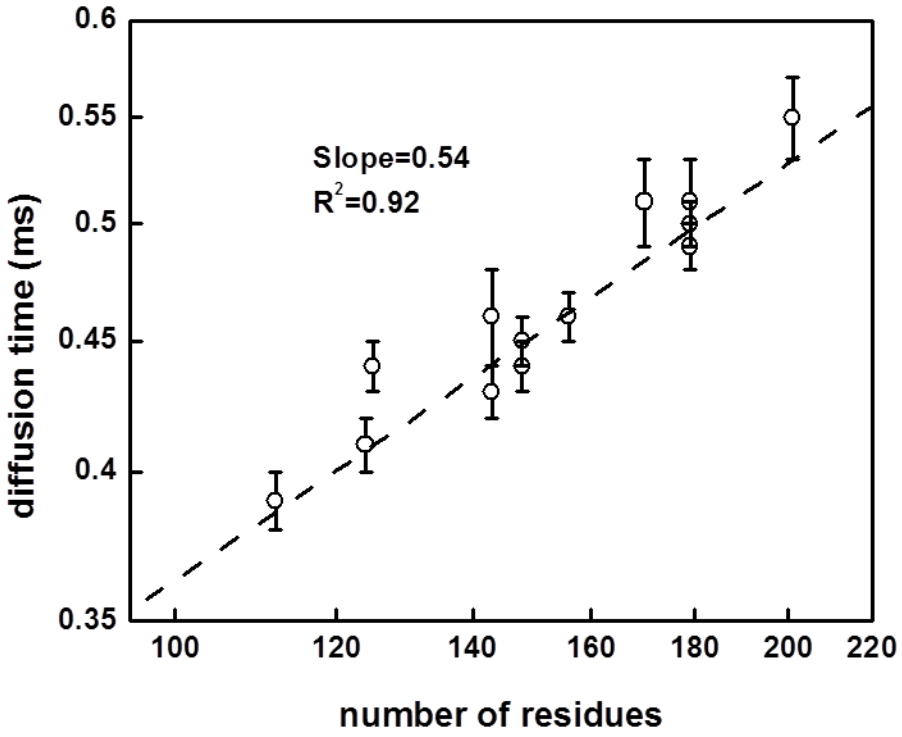

Figure S4 Diffusion times for tau constructs in solution. There is a linear correlation between diffusion time and size of the construct on a log-log scale. The scaling factor of 0.54 corresponds well to predicted values for random coil polymers (12).

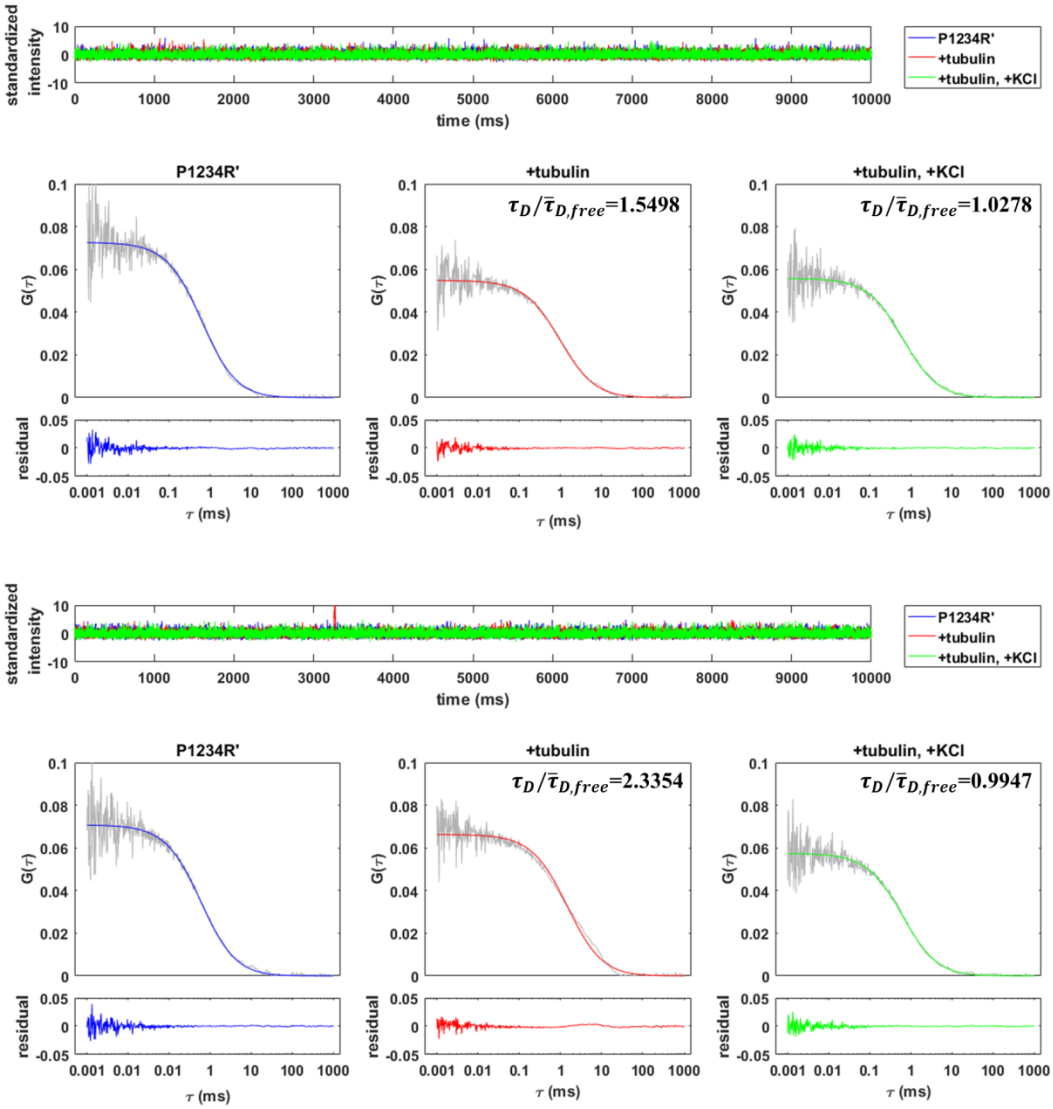

Figure S5 Representative photon traces for P1234R' in the absence (blue) or presence (red) of tubulin or tubulin + KCl (green). In the upper row, no low intensity bursts, as described in the text, are observed in the presence of tubulin, whereas in the lower row, bursts are observed. These events are only observed when both tau and tubulin are present (red). As increase in diffusion time is observed when tubulin is added to tau (red), independent of whether bursts are identified. The addition of 500 mM KCl to tau-tubulin mixtures (green) eliminates the bursting events and restored the autocorrelation curve to that of P1234R' in solution. The diffusion times in the second and third panels of both rows are relative to the diffusion time of P1234R' to better illustrate the changes.

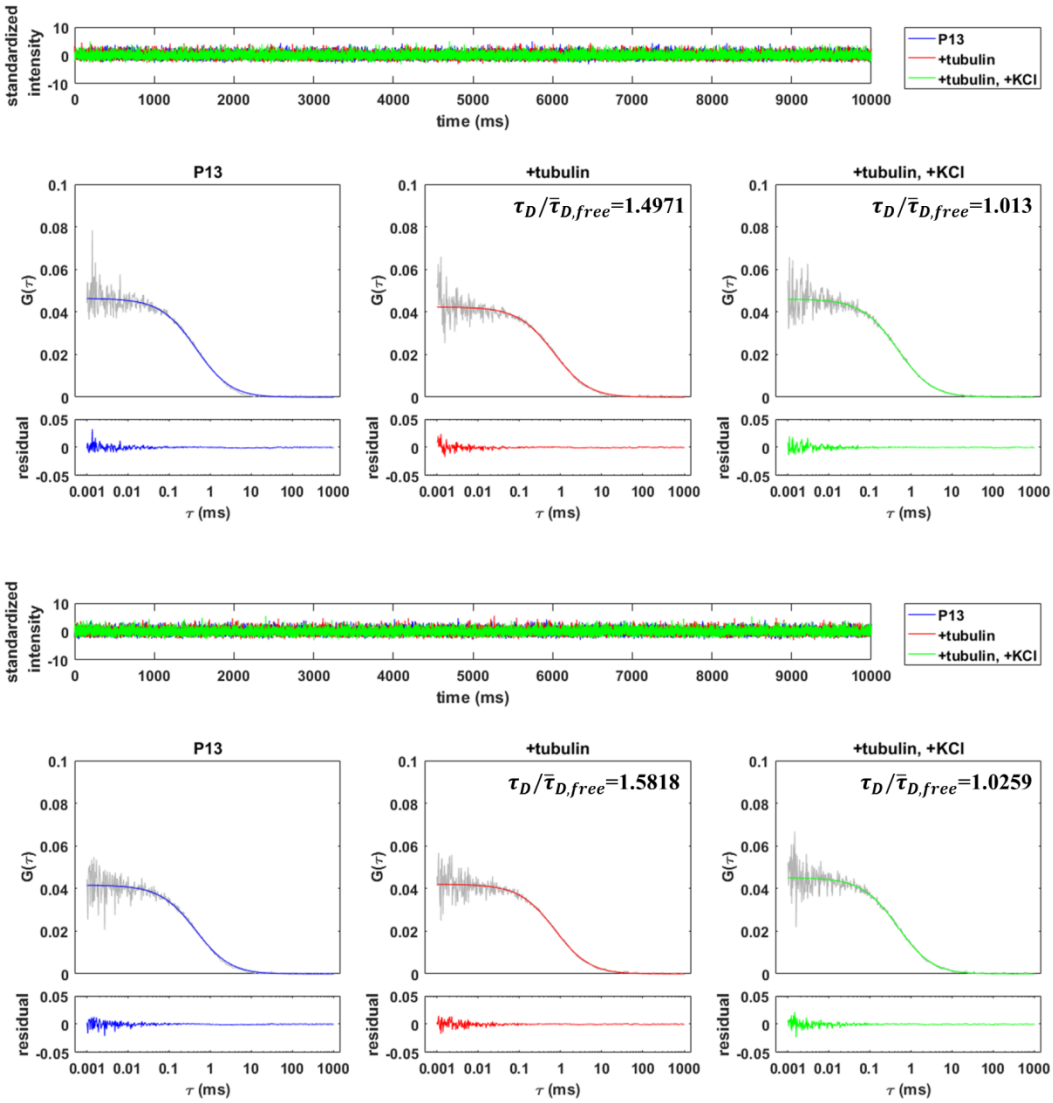

Figure S6 Representative photon traces for P13 in the absence (blue) or presence (red) of tubulin or tubulin + KCl (green). No low intensity bursts were identified for P13 by this analysis. As with P1234R', an increase in the diffusion time is seen upon the addition of tubulin (red) that decreases to that of tau in solution upon the addition of 500 mM KCl to tau-tubulin mixtures (green). The diffusion times in the second and third panels of both rows are relative to the diffusion time of P13 to better illustrate the changes.

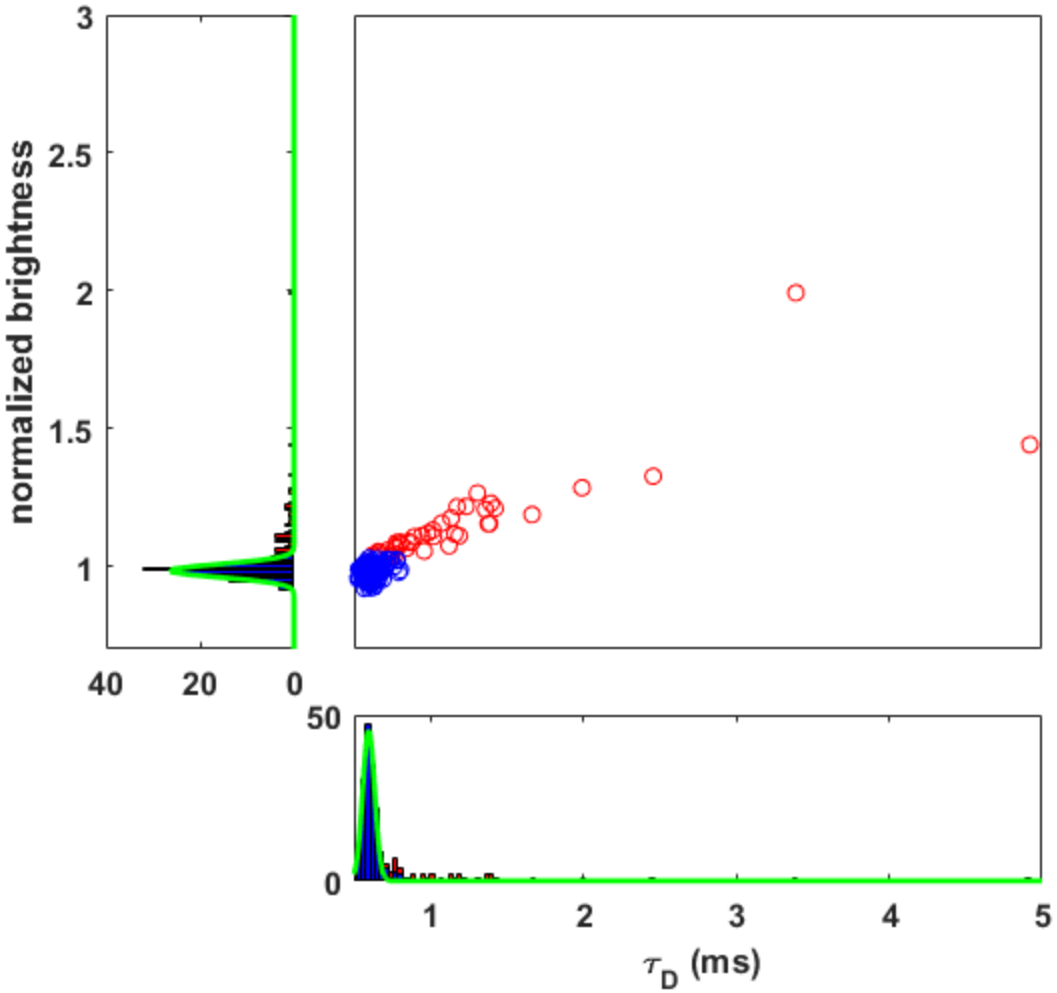

Figure S7 Graphical representation of brightness filtering for heterogeneous FCS. The 2D scatter plot shows the diffusion time and normalized molecular brightness for 200 individual autocorrelation curves. The red points were discarded through the iterative brightness analysis described in the text, while the blue points are the data used for further analysis. Histograms of the same data are shown along each axis with Gaussian fits in green

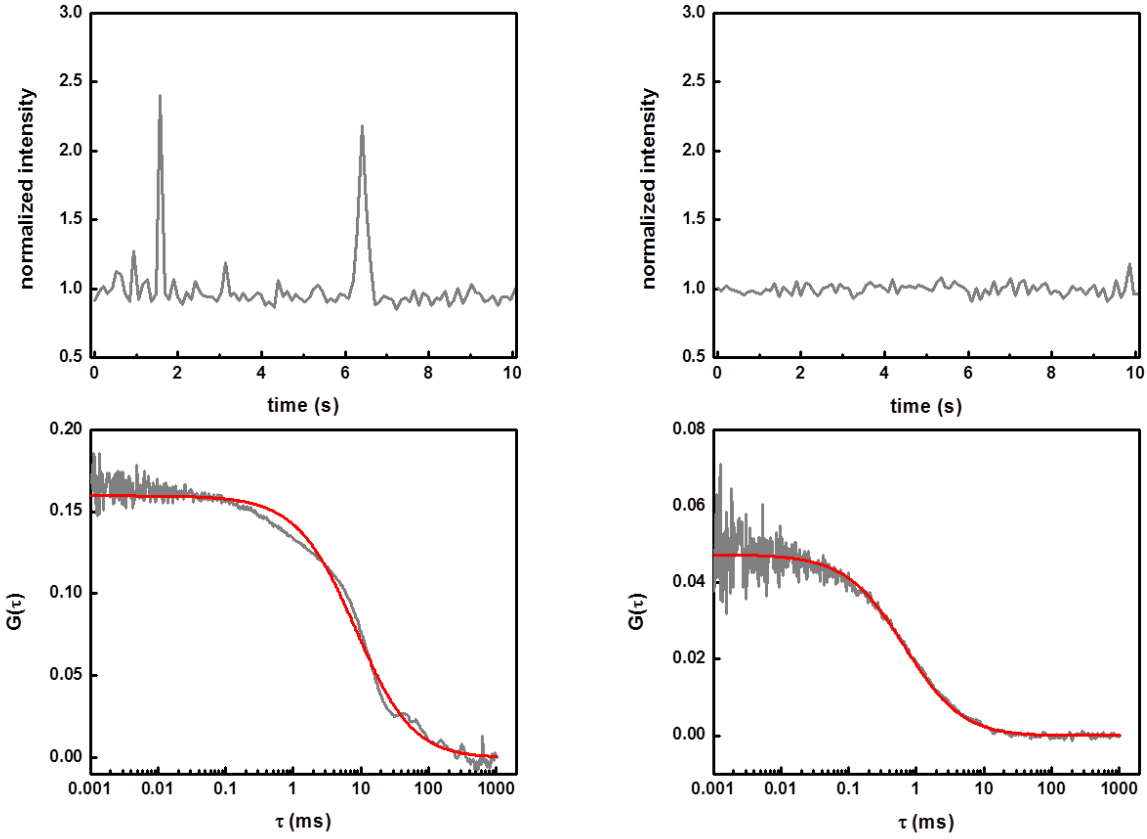

Figure S8 Representative autocorrelation curve caused by occasional sampling of very bright species (left) which is discarded during the Gaussian filtering as a result of increase of average molecular brightness of the autocorrelation curve. A measurement lacking these bright species is shown on the right for comparison. The autocorrelation curves are in gray, with single-component fits in red.

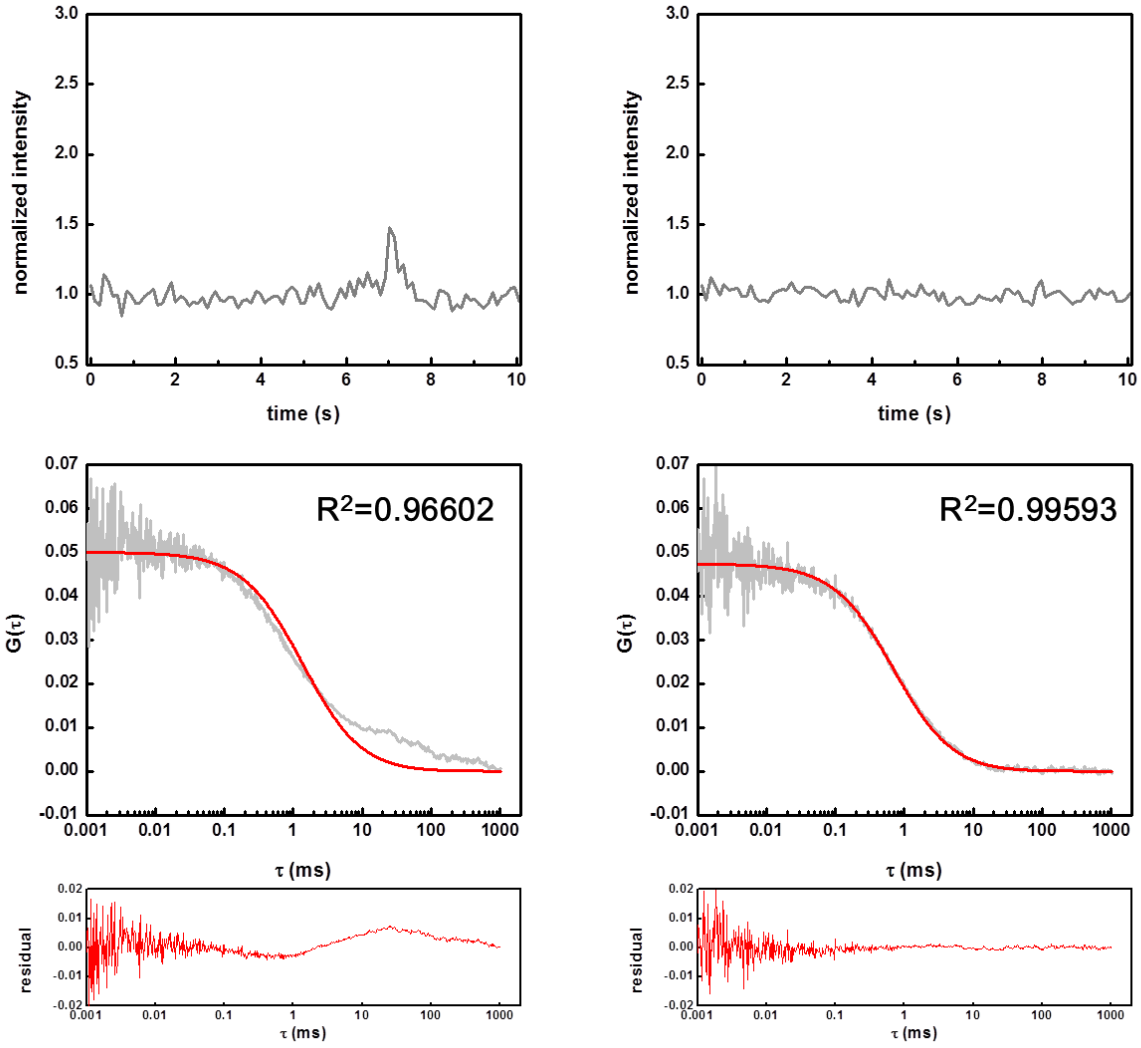

Figure S9 Sample showing abnormal time trace and autocorrelation curve caused by occasional sampling of less bright assemblies (left) which is discarded during the check of goodness of fitting. For comparison, an autocorrelation curve which was not eliminated in filtering is shown on the right. Gray curves are normalized intensity time traces (upper) and the autocorrelation curves (middle); red curves show the single-component fit of the autocorrelation curves (middle) and residuals (lower). R-squared is calculated for single-component fitting between 0.01 to 1000ms.

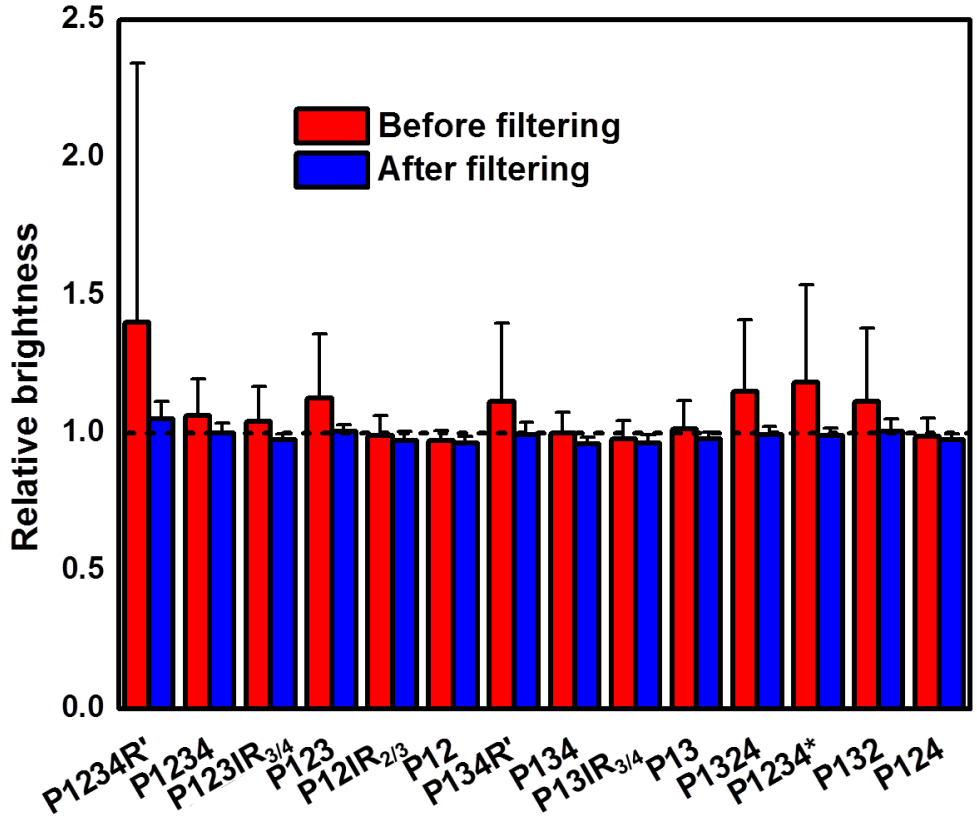

Figure S10 Molecular brightness of tau-tubulin complexes. The mean and standard deviation of molecular brightness before (red) and after (blue) data filtering by molecular brightness and goodness of fitting as described in the text are shown. The black dashed line denotes a relative brightness normalized to tau in solution.

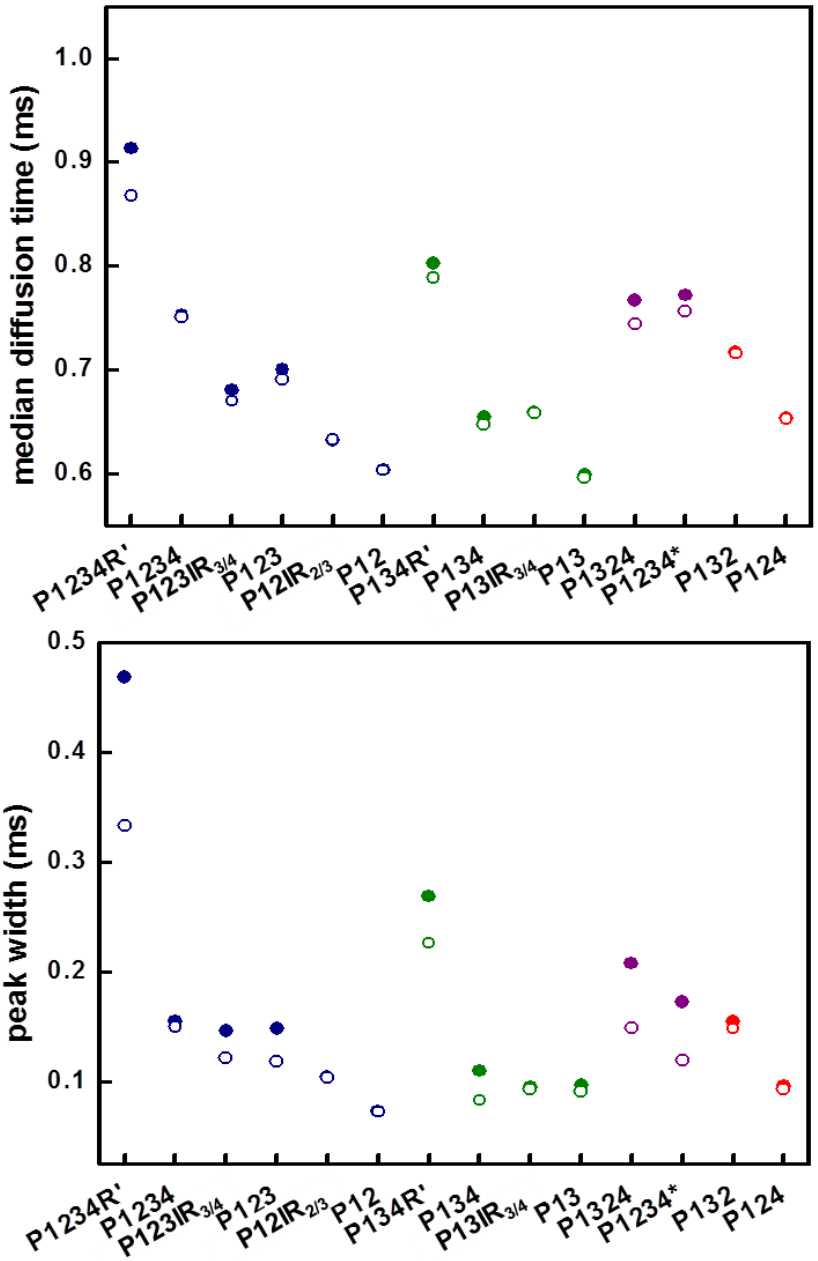

Figure S11 Comparison of median diffusion time and peak width from Gaussian fits prior to (filled circle) and following (empty circle) filtering by molecular brightness and goodness of fit. Although the absolute value for both parameters decrease after filtering, as the result of discarding high-brightness events, the relative relationship of complex size and heterogeneity between different constructs are retained. These data are colored as in Figures 2–4 in the manuscript: 4R series (blue); 3R series (green); scrambled series with 4 (purple) or 3 (red) repeats.

References:

1. Li, X.-H., J. A. Culver, and E. Rhoades. 2015. Tau binds to multiple tubulin dimers with helical structure. J. Am. Chem. Soc. 137:9218-9221.

2. Pecqueur, L., C. Duellberg, B. Dreier, Q. Y. Jiang, C. G. Wang, A. Pluckthun, T. Surrey, B. Gigant, and M. Knossow. 2012. A designed ankyrin repeat protein selected to bind to tubulin caps the microtubule plus end. Proc. Natl. Acad. Sci. USA 109:12011-12016.

3. Castoldi, M., and A. V. Popov. 2003. Purification of brain tubulin through two cycles of polymerization–depolymerization in a high-molarity buffer. Protein. Express. Purif. 32:83-88.

4. Hyman, A., D. Drechsel, D. Kellogg, S. Salser, K. Sawin, P. Steffen, L. Wordeman, and T. Mitchison. 1991. Preparation of modified tubulins. In Methods. Enzymol. B. V. Richard, editor. Academic Press. pp. 478-485.

5. Levy, S. F., A. C. LeBoeuf, M. R. Massie, M. A. Jordan, L. Wilson, and S. C. Feinstein. 2005. Three- and four-repeat tau regulate the dynamic instability of two distinct microtubule subpopulations in qualitatively different manners - implications for neurodegeneration. J. Biol. Chem. 280:13520-13528.

6. Hawkins, T. L., M. Mirigian, J. Li, M. S. Yasar, D. L. Sackett, D. Sept, and J. L. Ross. 2012. Perturbations in microtubule mechanics from tubulin preparation. Cell. Mol. Bioeng. 5:227-238.

7. Huang, N.-P., R. Michel, J. Voros, M. Textor, R. Hofer, A. Rossi, D. L. Elbert, J. A. Hubbell, and N. D. Spencer. 2001. Poly(L-lysine)-g-poly(ethylene glycol) layers on metal oxide surfaces:surface-analytical characterization and resistance to serum and fibrinogen adsorption. Langmuir. 17:489-498.

8. Meseth, U., T. Wohland, R. Rigler, and H. Vogel. 1999. Resolution of fluorescence correlation measurements. Biophys. J. 76:1619-1631.

9. Elbaum-Garfinkle, S., G. Cobb, J. T. Compton, X.-H. Li, and E. Rhoades. 2014. Tau mutants bind tubulin heterodimers with enhanced affinity. Proc. Natl. Acad. Sci. USA 111:6311-6316.

10. Holehouse, A. S., R. K. Das, J. N. Ahad, M. O. G. Richardson, and R. V. Pappu. 2016. CIDER: Resources to analyze sequence-ensemble relationships of intrinsically disordered proteins. Biophys. J. 112:16-21.

11. Das, R. K., and R. V. Pappu. 2013. Conformations of intrinsically disordered proteins are influenced by linear sequence distributions of oppositely charged residues. Proc. Natl. Acad. Sci. USA 110:13392-13397.

12. Hofmann, H., A. Soranno, A. Borgia, K. Gast, D. Nettels, and B. Schuler. 2012. Polymer scaling laws of unfolded and intrinsically disordered proteins quantified with single-molecule spectroscopy. Proc. Natl. Acad. Sci. USA 109:16155-16160.